Progress In Electromagnetics Research M, Vol. 106, 117–125, 2021

Validation of Grating Lobe Reductions in a Dual-Mode Scanning Phased Array Antenna

Zabed Iqbal, Tanzeela H. Mitha, and Maria Pour*

Abstract—The experimental validation of reduced grating lobes in a seven-element, hexagonal, scanning phased array antenna with the one-wavelength element spacing is presented. The base element of the array is a single-layer, dual-mode antenna with self-scanning and nulling properties. For the selected scan angle of $-30°$, the required microstrip transmission line based feeding network, consisting of ring hybrids, power splitters, and branchline couplers, are designed and developed. A prototype of the complete array and feeding network was fabricated and successfully tested to show the effectiveness of the grating lobe reduction method using the dual-mode antenna elements in scanning phased array antennas with the one-wavelength element spacing.

1. INTRODUCTION

Recently, much attention has been paid to the design and implementation of adaptive phased array antenna systems, intended for the use in satellite communications, ground terminals, unmanned vehicles, and wireless networks [1]. The motivation to use such adaptive phased arrays is to increase the scanning capability and improve the performance of wireless systems with a reduced number of elements and cost [2]. The design and implementation of scanning phased array antennas with a reduced number of antenna elements has been limited by a variety of factors. The primary hindrance of wide-scan deployment of phased array is the grating lobe generation in the visible region, which occurs when the inter-element spacing is greater than half a wavelength [3]. Several design methods have been proposed over the years to reduce grating lobes. Array thinning [4, 5] is one of the most common approaches to reduce grating lobes. Another solution is to use aperiodic distribution of the elements [6] or subarrays [7–9] with a tapered amplitude excitation [10]. Moreover, methods based on array element shaping [11], subarray quantization [12], mode-matching [13] and virtual filling [14] were reported to reduce grating lobes. However, all of the aforementioned grating lobe reduction methods and array syntheses use conventional single-mode antennas as the base element.

Recently, a novel adaptive dual-mode antenna element with unique self-scanning and self-nulling properties was effectively utilized to reduce grating lobe in a hexagonal phased array antenna by the authors in [15], where only analytical investigation and numerical results were reported. In this article, the newly established concept of grating lobes based on the utilization of these dual-mode antenna elements is validated through fabricating and testing a prototype phased array antenna in practice. In particular, a seven-element hexagonal planar scanning phased array, consisting of single-layer, dual-mode antenna elements [16], is designed, fabricated and tested for the scan angle of $-30°$ with the one-wavelength element spacing. To this end, the required feeding network was also fabricated and successfully tested to validate the grating lobe reduction method in practice.

Received 29 September 2021, Accepted 7 December 2021, Scheduled 17 December 2021
* Corresponding author: Maria Pour (maria.pour@uah.edu).
The authors are with the Department of Electrical and Computer Engineering, The University of Alabama in Huntsville, Huntsville, AL 35899, USA.

2. BASE ELEMENT AND SEVEN-ELEMENT HEXAGONAL PHASED ARRAY

For the assembly and handling purposes, the operating frequency of the array presented in [15] at 10 GHz is scaled down to 6 GHz. The hexagonal phased array is composed of seven dual-mode antenna elements with self-scanning and nulling properties. Unlike the dual-mode circular patch antenna element with a stacked configuration used in [15], which increases the fabrication complexities, herein a single-layer, dual-mode circular microstrip patch antenna [16] is adopted and rescaled for the 6 GHz operation as the base element of the scanning phased array. This single layer, dual-mode microstrip patch antenna significantly relaxes the fabrication, assembly and measurement processes. The geometry of the array and its dual-mode element is illustrated in Fig. 1. The elements are spaced one wavelength apart. The array is designed on the Rogers RO3003 substrate with the thickness of 1.53 mm and dielectric constant of 3. Each antenna element consists of a circular disc in the center, exciting the TM_{11} mode, and a concentric shorted ring patch encompassing the circular disc, exciting the TM_{21} mode.

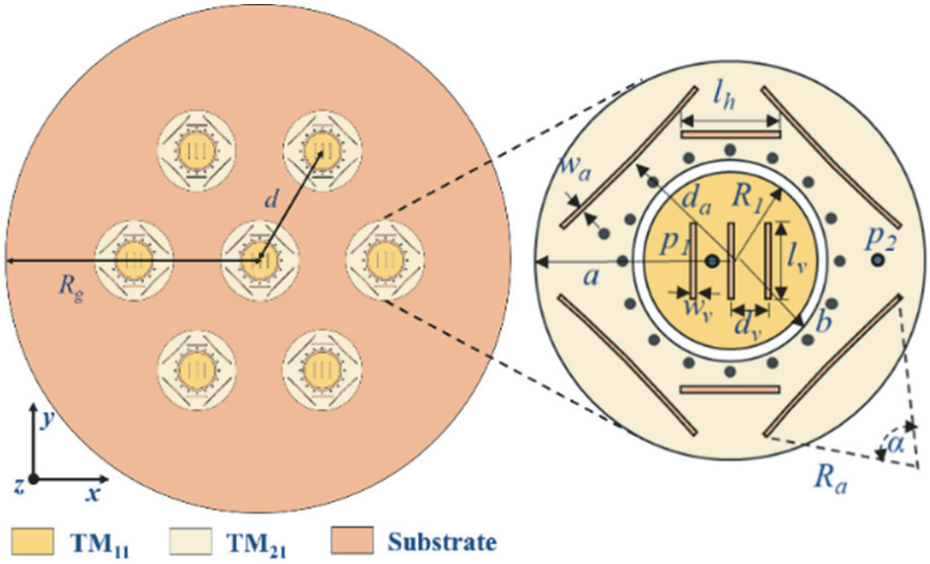

Figure 1. Top view of the seven-element single-layer hexagonal phased array with the element spacing $d = \lambda_o$, $R_g = 2\lambda_o$; λ_o is the free space wavelength at 6 GHz. (Inset: Top view of the dual-mode single-layer antenna element [16] rescaled to 6 GHz with $R_1 = 7.28$ mm, $a = 15.9$ mm, $b = 8.07$ mm, $l_v = 6$ mm, $d_v = 3.6$ mm, $d_a = 11.71$ mm, $l_h = 7.2$ mm, $R_a = 60$ mm, $\alpha = 11.95°$, the TM_{11} and TM_{21} modes are excited by probes p_1 and p_2 in each element, respectively.)

As shown in Fig. 1, the proposed phased array has a hexagonal configuration with one central and six peripheral elements distributed evenly over a circle of radius $d = \lambda_o$, where λ_o is the free space wavelength at 6 GHz. As detailed in [15], an amplitude tapering (w) of the peripheral elements is required to reduce the grating lobe effectively along with the utilization of self-scanning and self-nulling properties of the dual-mode antenna elements. The required amplitude tapering is equal to unity ($w = 1$ or 0 dB) for the central element and $w = 0.375$ (−8.5 dB) for the six peripheral elements.

3. FEEDING NETWORK

To scan the array main beam, proper phase shifts need to be applied to the antenna elements and their modes. Moreover, the amplitude tapering is also required to reduce the grating lobes. To fulfill all these, a 1 : 14 planar feeding network based on the microstrip transmission line is designed by incorporating two ring hybrids [17], two three-way power dividers [18], and seven branchline couplers [17] as shown in Fig. 2. The complete feeding network is a 28-port structure capable of producing the required power ratios and phase shifts to feed the seven-element phased array antenna to scan the main beam to −30°.

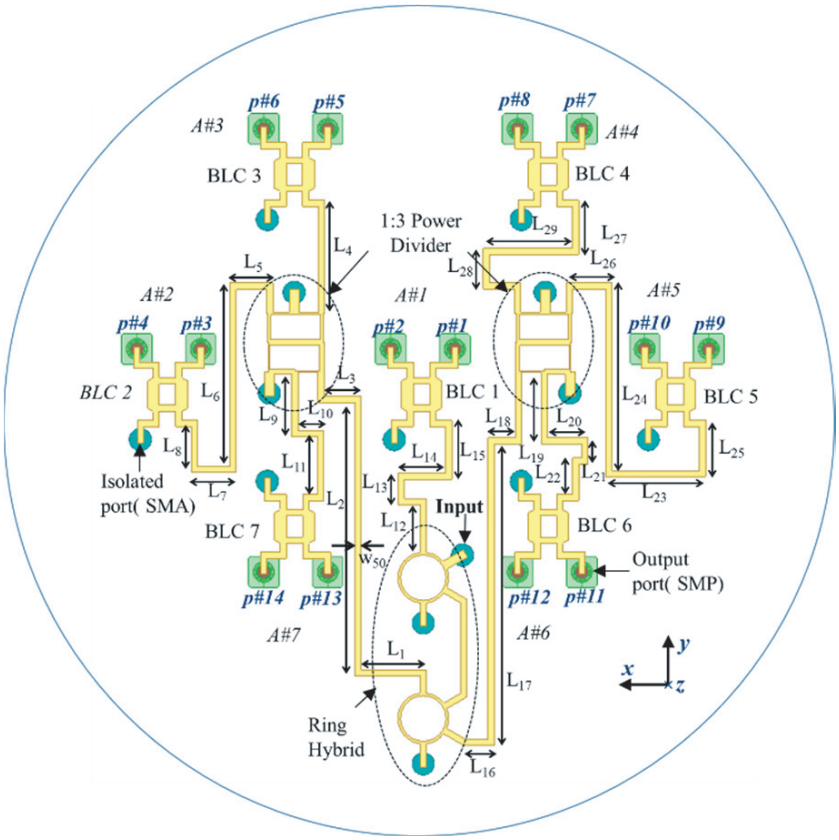

Figure 2. Top view of the feeding network designed at 6 GHz on a 1.28 mm-thick Rogers RO3010 substrate (transparent), when $L_1 = 12.85$ mm, $L_2 = 53.85$ mm, $L_3 = 7.3$ mm, $L_4 = 22.25$ mm, $L_5 = 8.5$ mm, $L_6 = 36$ mm, $L_7 = 8.72$ mm, $L_8 = 9$ mm, $L_9 = 12.35$ mm, $L_{10} = 5.06$ mm, $L_{11} = 11.3$ mm, $L_{12} = 9.38$ mm, $L_{13} = 6.2$ mm, $L_{14} = 9.36$ mm, $L_{15} = 11.6$ mm, $L_{16} = 6$ mm, $L_{17} = 59.33$ mm, $L_{18} = 5.35$ mm, $L_{19} = 14$ mm, $L_{20} = 7.92$ mm, $L_{21} = 5.17$ mm, $L_{22} = 7.17$ mm, $L_{23} = 19.65$ mm, $L_{24} = 36.96$ mm, $L_{25} = 11.12$ mm, $L_{26} = 9$ mm, $L_{27} = 10.65$ mm, $L_{28} = 8$ mm, $L_{29} = 17.58$ mm, and $w_{50} = 1.2$ mm.

Out of the 28 ports, 14 ports are output ports to be used as feeding points for the seven-element dual-mode phased array, one port is the input, and the remaining 13 ports are the isolated ports, which are matched with the 50 Ω loads.

The 28-port feeding network was full-wave analyzed in ANSYS HFSS [19]. The power in output ports #3 to #14 is approximately 8.5 dB less than the output ports #1–2, which is equivalent to the required amplitude tapering of $w = 0.375$ for the peripheral elements, as per Fig. 3. This amplitude distribution is close to our analytical prediction reported in [15]. Fig. 3(a) depicts the delivered power, relative to the input port, at the TM_{11} output ports ($p\#i$, where, $i = 1$, 3, 5, 7, 9, 11, and 13) that are designated to excite the TM_{11} patches in the array. Similarly, Fig. 3(b) represents the relative power delivered to the TM_{21} output ports ($p\#i$, where, $i = 2$, 4, 6, 8, 10, 12, and 14). It is seen that the difference between the power delivered to the central element ($p\#1$ and $p\#2$) to the peripheral elements ($p\#3$ to $p\#14$) is about 8–9 dB. Phase responses of the feeding network are illustrated in Figs. 4(a)–(b) for the TM_{11} and TM_{21} ports relative to the input port. As observed, the difference between TM_{11} ($p\#i$) to TM_{21} ($p\#i$) is about 80°. It should be noted that a 90° phase shift between the two modes would be ideally needed as reported in [15] based on the cavity model. However, the 80° phase shift was found to be optimal in the full-wave analysis due to the probe effects and their asymmetric placements in each element. Moreover, the relative phase response of the output ports is within ±5° margin of error to that of the required phase to scan the beam to −30°, as listed in Table 1.

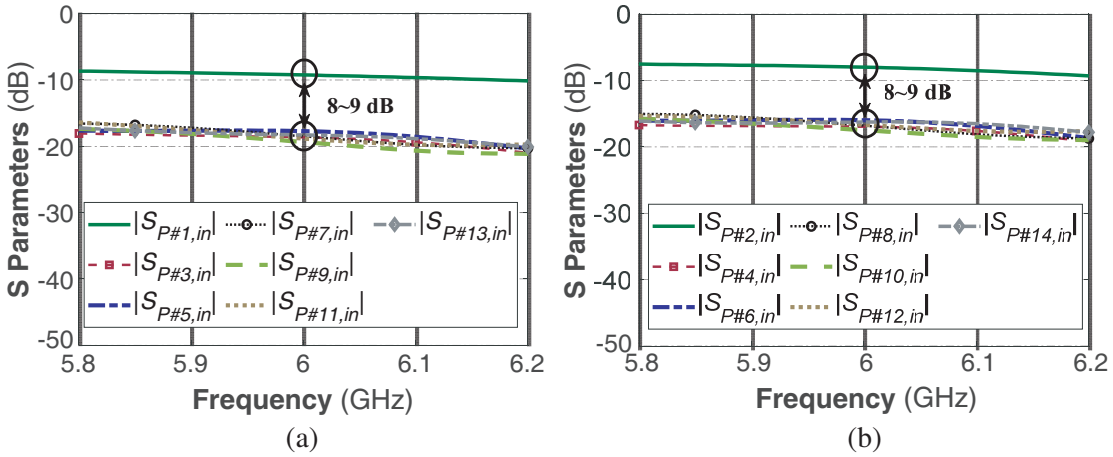

Figure 3. Simulated S-parameters representing amplitude tapering between (a) central elements ($p\#1$: TM_{11}) to peripheral elements TM_{11} ports, (b) central elements ($p\#2$: TM_{21}) to peripheral elements TM_{21} ports.

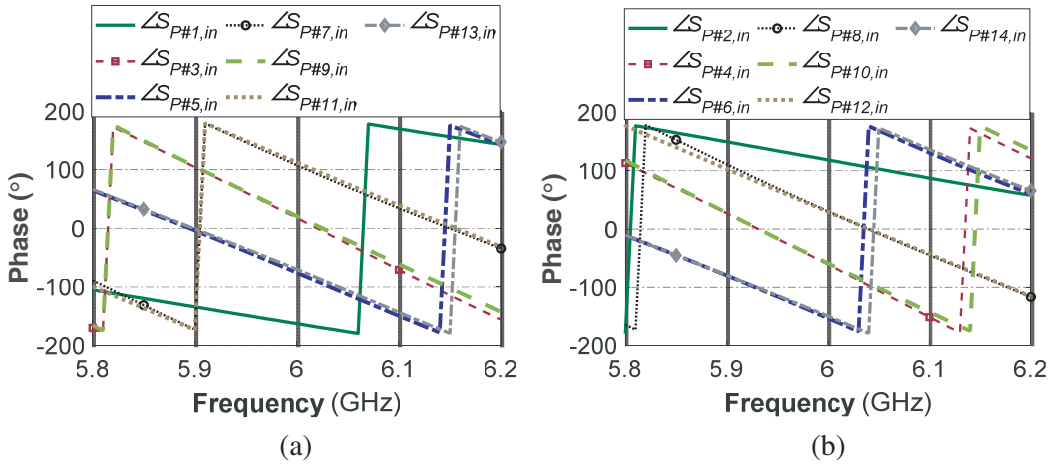

Figure 4. Simulated phase response of the (a) TM_{11}, (b) TM_{21} ports of the feeding network.

Table 1. Comparison of the required and simulated phase response of the feeding network to scan the array main beam to $-30°$, [Phase unit: degrees].

Antenna	Required Phase to scan $-30°$		Normalized Simulated Phase			Phase Errors	
	TM_{11} ports	TM_{21} ports	TM_{11} ports	TM_{21} ports	Diff.	TM_{11} ports	TM_{21} ports
A1	0	-80	0	-78.89	-78.89	**0**	**1.11**
A2	-180	-260	-179.9	-258.5	-78.57	**0.07**	**1.5**
A3	-270	-350	-273.1	-350.5	-77.41	**3.14**	**0.55**
A4	-90	-170	-89.76	-167.1	-77.35	**0.24**	**2.89**
A5	-180	-260	-176.6	-256.5	-79.85	**3.34**	**3.49**
A6	-90	-170	-85.27	-167.9	-82.72	**4.73**	**2.01**
A7	-270	-350	-267.5	-347.1	-79.6	**2.47**	**2.87**

4. COMPLETE SINGLE-LAYER, DUAL-MODE, SEVEN-ELEMENT HEXAGONAL ARRAY

A complete scanning phased array was full-wave analyzed in ANSYS HFSS [19] by combining the seven-element, single-layer phased array with the designed feeding network at the center frequency of 6 GHz. The feeding network was placed under the hexagonal array and connected to the input ports of the array with SMP (Sub miniature push-on) connectors and SMP compatible adapters, as shown in Fig. 5. The distance between each element is λ_o and the overall diameter of the phased array antenna is $4\lambda_o$, where λ_o is the free-space wavelength at 6 GHz. The simulated results of the single-layer, dual-mode, seven-element hexagonal array with the feeding network are compared with the measured ones in Section 5.

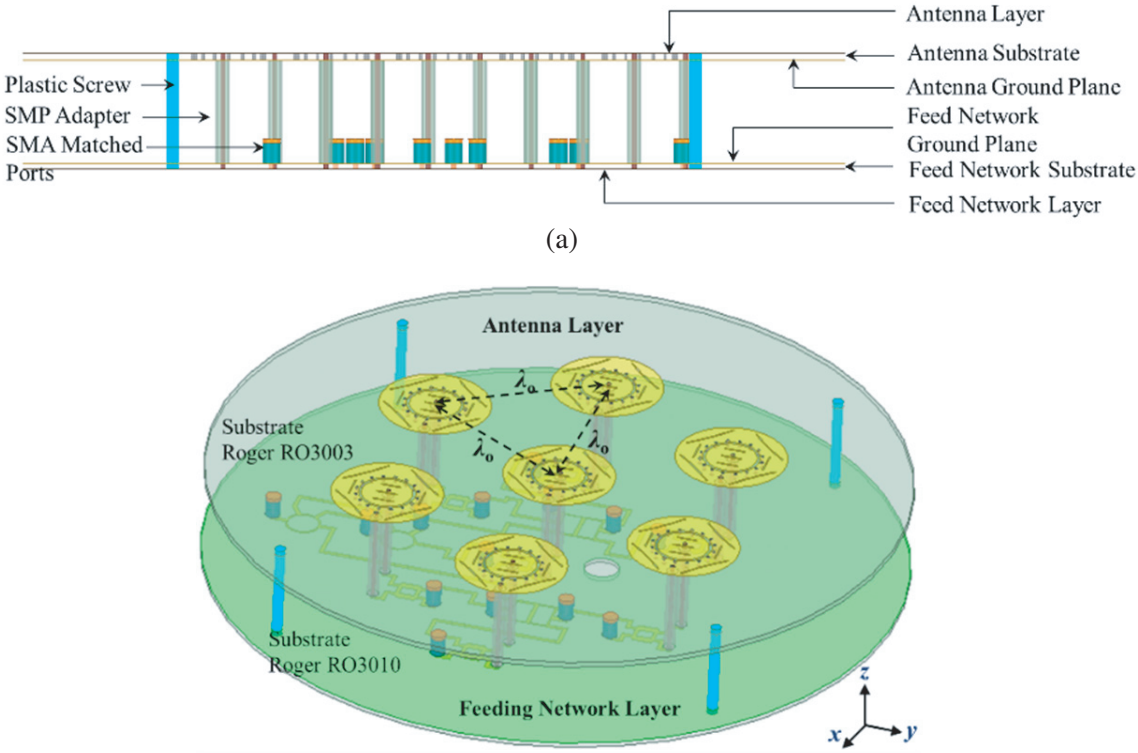

Figure 5. (a) Side view and (b) perspective view of the seven-element hexagonal phased array with the complete feeding network, when element spacing is a free space wavelength at 6 GHz ($\lambda_o = 50$ mm).

5. MEASUREMENT RESULTS

A prototype of the seven-element, dual-mode scanning phased array and the feeding network, illustrated in Fig. 6, was fabricated and tested to validate the numerical results in practice. The radiation pattern measurements were conducted in the spherical near-field anechoic chamber of the University of Alabama in Huntsville, as shown in Fig. 6(c).

The S-parameters of the individual element of the fabricated phased array were measured using a two-port vector network analyzer. These S-parameters include the reflection coefficients at each dual-mode element and coupling between the elements. Fig. 7 depicts the S-parameters of the central element (A1), while the remaining elements are terminated with the 50 Ω loads. As observed, the measured and simulated reflection coefficients of TM_{11} patch (S_{11}) and isolation between TM_{11} and TM_{21} patches ($S_{12} = S_{21}$) are in good agreement, whereas the measured reflection coefficient of TM_{21} patch is slightly shifted to 5.96 GHz from 6 GHz. Nonetheless, the measured $|S_{22}|$ is still less than -10 dB at 6 GHz.

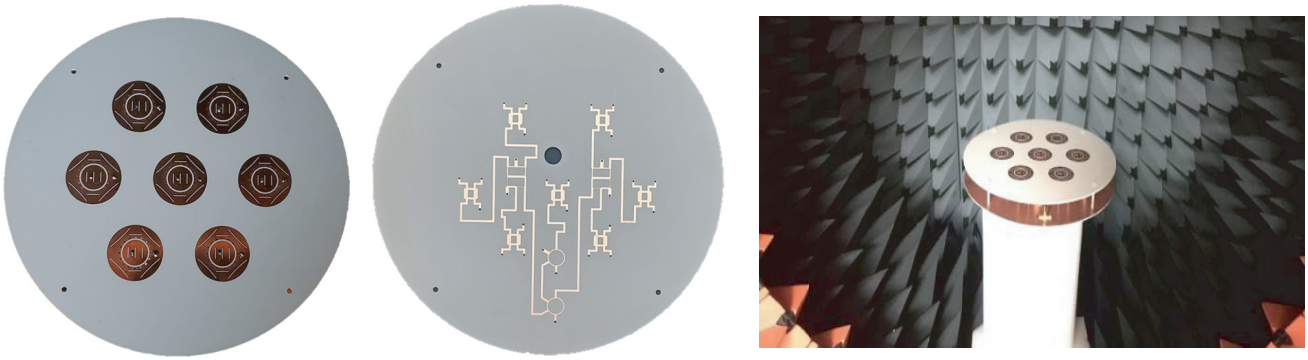

(a) (b) (c)

Figure 6. Photographs of (a) the fabricated seven-element, dual-mode hexagonal phased array antenna with one-wavelength element spacing, (b) fabricated feeding network and, (c) complete phased array antenna under test.

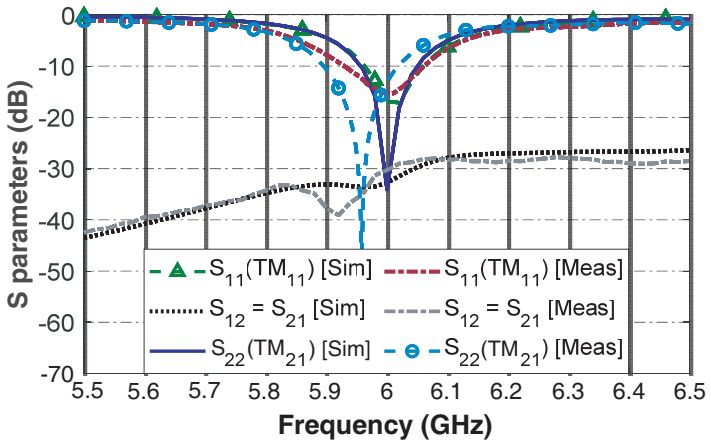

Figure 7. Measured and simulated S-parameters of the center element (A1) of the seven-element dual-mode phased array antenna.

The reflection coefficients and isolation between the modes in the peripheral dual-mode elements were also measured, which all exhibited the same trend. The mutual coupling between the TM_{11} and TM_{21} modes in all the seven elements is below -25 dB.

The mutual coupling between the elements of the fabricated phased array prototype was measured and compared with the simulated ones in Fig. 8. The maximum mutual coupling occurs between the adjacent TM_{21} to TM_{21} patches, which is about -20 dB as per Figs. 8(a)–(b). For all other groups, i.e., ($TM_{11} - TM_{21}$, $TM_{11} - TM_{11}$) in the adjacent elements, the mutual coupling is well below -20 dB. For the non-adjacent elements, mutual coupling is negligible, which is less than -30 dB at 6 GHz as shown in Fig. 8(c).

The radiation pattern measurements were conducted in two steps. First, the individual element patterns were measured with all other elements terminated with 50 Ω loads. With the hexagonal configuration, the active element patterns of A2 and A5 are similar and active element patterns of A3, A4, A6 and A7 follow a similar trend. As a representative example, the simulated and measured realized gain patterns of elements A1 and A4 at 6 GHz are plotted in Fig. 9, which are aligned very well for both modes.

Later, the feeding network was incorporated with the hexagonal phased array antenna, and the VSWR of the input port and the overall radiation pattern were measured. Both the measured and simulated VSWRs of the complete phased array antenna are plotted in Fig. 10. Due to the accumulated air gaps between the SMP adapters and SMP connectors, especially for the central element during the

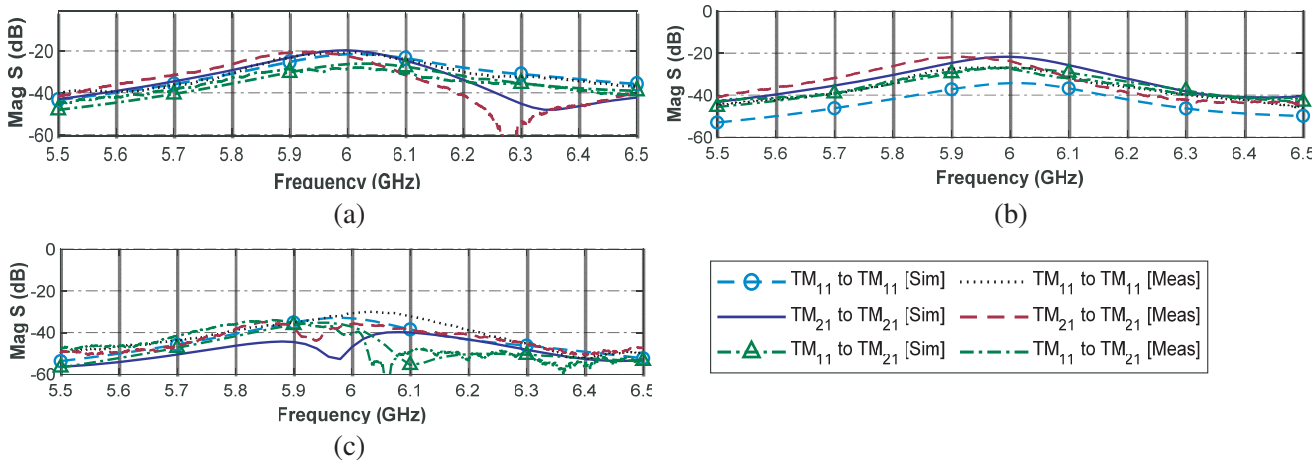

Figure 8. Measured and simulated S-parameters representing mutual coupling between (a) A1 to A2, (b) A2 to A3 (adjacent), (c) A2 to A4 (non-adjacent) elements of the seven-element hexagonal phased array antenna.

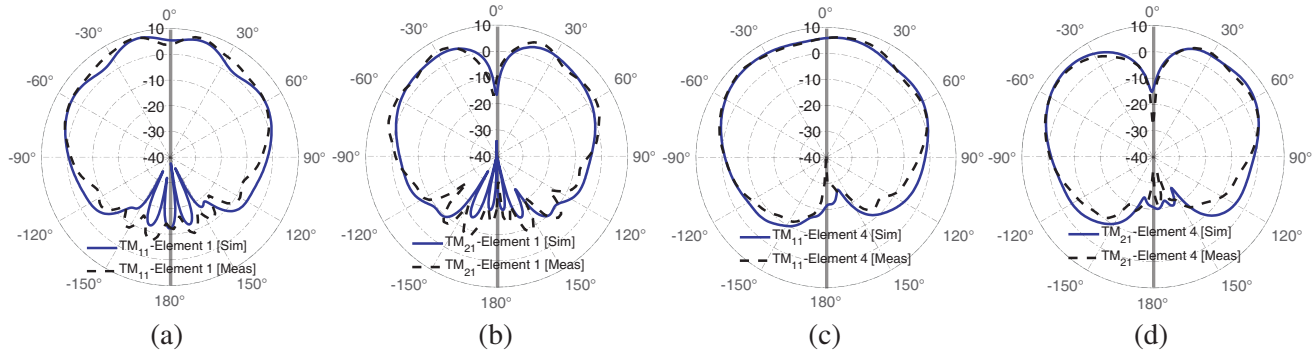

Figure 9. Measured and simulated active realized gain patterns of the (a)–(b) Element 1 (A1), and (c)–(d) Element 4 (A4) of the dual-mode seven-element hexagonal phased array at 6 GHz.

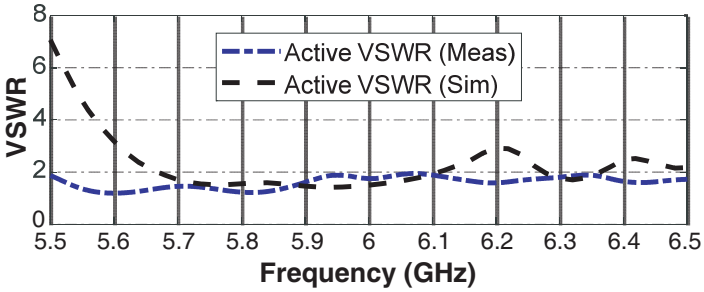

Figure 10. Measured and simulated *VSWR* of the input of the seven-element phased array antenna with the feeding network.

manual assembly and the compression caused by the snap-on SMPs, the effective electrical lengths of the feeding transmission lines increased, leading to a slight shift in the operating frequency from 6 GHz to 5.8 GHz in the measurement to obtain the required phase shift for the $-30°$ scan angle. Hence, the grating lobe reduction capability of the fabricated phased array will be provided at the frequency of 5.8 GHz.

The measured radiation patterns at 5.8 GHz of the complete phase array with its feeding network

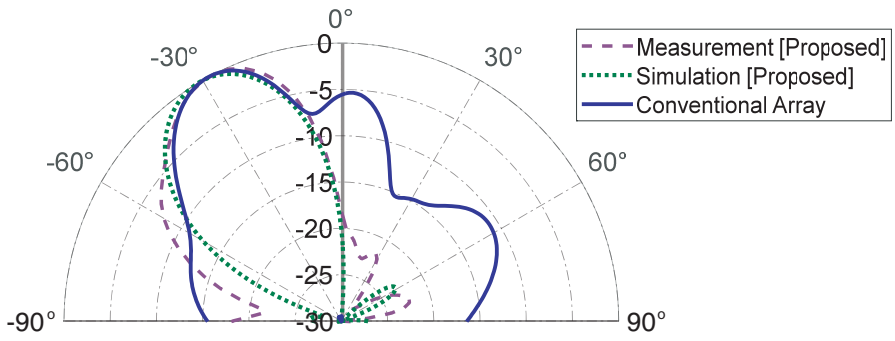

Figure 11. Normalized measured radiation pattern of the seven-element dual-mode hexagonal phased array at 5.8 GHz and simulated radiation patterns of the seven-element dual-mode (proposed) and conventional single-mode hexagonal array at 6 GHz with the $-30°$ scan angle and 1λ element spacing.

are shown in Fig. 11 and compared with the simulation results for both single- and dual-mode elements at 6 GHz for the $-30°$ scan angle in the E-plane. The results confirm the capability of the dual-mode ($TM_{11}+TM_{21}$) antenna elements to reduce the unwanted grating lobes with the one-wavelength element spacing. The radiation pattern of the seven-element, dual-mode hexagonal array is also compared with the reference case, which is a conventional seven-element hexagonal array consisting of only single-mode TM_{11} antenna elements with the one-wavelength element spacing. Both of the conventional single-mode and proposed dual-mode arrays are excited with the $w = 0.375$ amplitude distribution and identical phase shifts to scan the main beam to $-30°$. As observed, the grating lobe level for the reference case is quite high, close to -5 dB for the $-30°$ scan angle, as per Fig. 11. In contrast, for the proposed dual-mode case in both measurement and simulation, the grating lobe is reduced to -22 dB by utilizing the self-scanning and nulling properties of the dual-mode base elements.

6. CONCLUSION

The experimental validation of the grating lobe suppression in a hexagonal scanning array with the one-wavelength element spacing was addressed. The arrays comprising of conventional single-mode elements suffer from large grating lobes. It was shown that by utilizing dual-mode elements with self-scanning and adaptive nulling properties, the grating lobe could be reduced significantly. The designed dual-mode antenna was employed as a radiation-matched base element in the proposed seven-element hexagonal scanning phased array with the one-wavelength element spacing. The numerical results were validated through fabricating and testing a prototype phased array antenna in practice, along with its feeding network. This showcased the potential of the dual-mode antenna elements in the future generation of scanning phased array antennas with large element spacing.

ACKNOWLEDGMENT

This work was supported in part by the National Science Foundation (NSF) CAREER Award No. ECCS-1653915 and the Alabama Graduate Research Scholars Program (GRSP) round 15 and 16, funded through the Alabama Commission for Higher Education and administered by the Alabama EPSCoR.

REFERENCES

1. Fourikis, N., *Phased Array-Based Systems and Applications*, John Wiley & Sons, New York, 1997.
2. Mailloux, R. J., *Phased Array Antenna Handbook*, 2nd Edition, Artech House, Norwood, MA, USA, 2005.
3. Balanis, C. A., *Antenna Theory: Analysis and Design*, 4th Editoin, Wiley, Hoboken, 620 NJ, USA, 2016.

4. Helander, J., D. Tayli, and D. Sjoberg, "Multi-port element for grating lobe suppression in sparse VHF phased array radars," *IEEE Trans. Antennas Propag.*, Vol. 67, No. 10, 6667–6671, Oct. 2019.
5. Tu, X., G. Zhu, X. Hu, and X. Huang, "Grating lobe suppression in sparse array-based ultra-wideband through-wall imaging radar," *IEEE Antennas Wireless Propag. Lett.*, Vol. 15, 1020–1023, Oct. 2016.
6. Lu, B., S. X. Gong, S. Zhang, Y. Guan, and J. Ling, "Optimum spatial arrangement of array elements for suppression of grating-lobes of radar cross section," *IEEE Antennas Wireless Propag. Lett.*, Vol. 9, 114–117, Feb. 2010.
7. Bianchi, D., S. Genovesi, and A. Monorchio, "Randomly overlapped subarrays for reduced sidelobes in angle-limited scan arrays," *IEEE Antennas Wireless Propag. Lett.*, Vol. 16, 1969–1972, Apr. 2017.
8. Krivosheev, Y. V., A. V. Shishlov, and V. V. Denisenko, "Grating lobe suppression in aperiodic phased array antennas composed of periodic subarrays with large element spacing," *IEEE Antennas Propag. Magazine*, Vol. 57, No. 1, 76–85, Feb. 2015.
9. Brockett, T. J. and Y. R.-Samii, "Subarray design diagnostics for the suppression of undesirable grating lobes," *IEEE Trans. Antennas Propag.*, Vol. 60, No. 3, 1373–1380, Mar. 2012.
10. Haupt, R. L., "Reducing grating lobes due to subarray amplitude tapering," *IEEE Trans. Antennas Propag.*, Vol. 9, No. 8, 846–850, Aug. 1985.
11. Bavaro, V., G. Caliano, and M. Pappalardo, "Element shape design of 2-D CMUT arrays for reducing grating lobes," *IEEE Trans. Ultrason., Ferroelec., Freq. Contr.*, Vol. 55, No. 2, 308–318, Feb. 2008.
12. Hansen, R. C. and G. G. Charlton, "Subarray quantization lobe decollimation," *IEEE Trans. Antennas Propag.*, Vol. 47, No. 8, 1237–1239, Aug. 1999.
13. Skobelev, S. P. and P.-S. Kildal, "Blindness removal in arrays of rectangular waveguides using dielectrically loaded hard walls," *IEEE Trans. Antennas Propag.*, Vol. 46, No. 4, 546–550, Apr. 1998.
14. Feng, B.-K. and D. C. Jenn, "Grating lobe suppression for distributed digital subarrays using virtual filling," *IEEE Antennas Wireless Propag. Lett.*, Vol. 12, 1323-1326, Oct. 2013.
15. Iqbal, Z. and M. Pour, "Grating lobe reduction in scanning phased array antennas with large element spacing," *IEEE Trans. Antennas Propag.*, Vol. 66, No. 12, 6965–6974, Dec. 2018.
16. Iqbal, Z., T. Mitha, and M. Pour, "A self-nulling single-layer dual-mode microstrip patch antenna for grating lobe reduction," *IEEE Antennas Wireless Propag. Lett.*, Vol. 19, No. 9, 1506–1510, Sept. 2020.
17. Pozar, D. M., *Microwave Engineering*, Wiley, Hoboken, NJ, 2012.
18. Lim, J.-S. and S.-Y. Eom, "A new 3-way power divider with various output power ratios," *IEEE MTT-S International Microwave Symposium Digest*, Vol. 2, 785–788, San Francisco, CA, USA, Jun. 17–21, 1996.
19. *High Frequency Structure Simulator (HFSS 18.0),* Canonsburg, PA, USA, ANSYS, 2018.